IOP Publishing Physics in Medicine and Biology

Phys. Med. Biol. **52** (2007) 1633–1646 doi:10.1088/0031-9155/52/6/006

Temperature and SAR measurement errors in the evaluation of metallic linear structures heating during MRI using fluoroptic® probes

E Mattei[1], M Triventi[1], G Calcagnini[1], F Censi[1], W Kainz[2], H I Bassen[2] and P Bartolini[1]

[1] Department of Technologies and Health, Italian National Institute of Health, Roma, Italy
[2] Center for Devices and Radiological Health, Food and Drug Administration, Rockville, MD, USA

E-mail: eugenio.mattei@iss.it

Received 25 September 2006, in final form 8 January 2007
Published 26 February 2007
Online at stacks.iop.org/PMB/52/1633

Abstract

The purpose of this work is to evaluate the error associated with temperature and SAR measurements using fluoroptic® temperature probes on pacemaker (PM) leads during magnetic resonance imaging (MRI). We performed temperature measurements on pacemaker leads, excited with a 25, 64, and 128 MHz current. The PM lead tip heating was measured with a fluoroptic® thermometer (Luxtron, Model 3100, USA). Different contact configurations between the pigmented portion of the temperature probe and the PM lead tip were investigated to find the contact position minimizing the temperature and SAR underestimation. A computer model was used to estimate the error made by fluoroptic® probes in temperature and SAR measurement. The transversal contact of the pigmented portion of the temperature probe and the PM lead tip minimizes the underestimation for temperature and SAR. This contact position also has the lowest temperature and SAR error. For other contact positions, the maximum temperature error can be as high as −45%, whereas the maximum SAR error can be as high as −54%. MRI heating evaluations with temperature probes should use a contact position minimizing the maximum error, need to be accompanied by a thorough uncertainty budget and the temperature and SAR errors should be specified.

1. Introduction

Magnetic resonance imaging (MRI) is a widely accepted tool for the diagnosis of a variety of disease states. However, the presence of a metallic implant, such as a cardiac pacemaker, or the use of conductive structures in interventional therapy, such as guide wires or catheters, are currently considered a strong contraindication to MRI (Niehaus and Tebbenjohanns 2001,

Pinski and Trohman 2002, Kanal *et al* 2002, Shellock and Crues 2002). Most of the publications dealing with novel MR techniques on patients with implanted linear conductive structures (Dumoulin *et al* 1993, Leung *et al* 1995, Glowinsky *et al* 1997, Atalar *et al* 1998, Baker *et al* 2004) point out that the presence of these structures may produce an increase in power deposition around the wire or the catheter. Unfortunately, this increased local absorption rate (SAR) is potentially harmful to the patient due to an excessive temperature increase which can bring living tissues to necrosis. The most direct way to measure SAR deposition along the wire is by using a fluoroptic® temperature probe. In such probes, the temperature sensor is a half-sphere of approximately a 0.3 mm diameter encapsulated inside a cylindrical pigmented jacket and located at the terminal portion of a flexible fibre optic cable. The pigmented jacket (approx. 3 mm length, 0.8 mm diameter) has to prevent ambient light from interfering with the sensor, as well as acting as a reference for the probe positioning.

Because of the well-known limitations of conventional thermometry methods in radiofrequency energy environments (Wickersheim and Sun 1987, Shellock 1992), the use of fluoroptic® thermometry has become the 'state-of-the-art' and the industry standard in this field. This method has been used to examine radiofrequency energy-induced heating of tissues, *in vitro* and *in vivo* (Blouin *et al* 1991, Shellock 1992, Shellock *et al* 1994, Dinerman *et al* 1996, Shellock and Shields 2000).

However, some methodological issues have found limited attention so far. Among them, the underestimation of heating due to the positioning of the temperature probes, as well as the error in temperature and SAR measurement needs to be investigated and standardized. In particular, thin linear structures such as PM leads may generate temperature gradients which cannot be neglected with respect to the physical dimension of the temperature probes. As a consequence, it is not possible to obtain accurate estimation of the maximum temperature and SAR in the lead tip region. When the investigation involves small objects and rapidly changing (in space and time) temperature gradients, there is the need to define a standardized method for positioning of the temperature probes. This standardized method should minimize the underestimation and the error associated with temperature and SAR measurements. In most of the publications dealing with the heating of conductive structure during MRI, the generated heat is confined in close proximity to the lead tip, but temperature increases appear significantly different, even in the case of apparently similar experimental set-ups (Achenbach *et al* 1997, Sommer *et al* 2000, Nitz *et al* 2001, Ruggera *et al* 2003, Roguin *et al* 2004). The relative positioning of the temperature probe and the lead tip may significantly affect the measurement and can explain, at least partially, the inconsistency of the results.

The aim of this paper is to identify a positioning of fluoroptic® temperature probes next to PM lead tips to measure the maximum lead tip heating. Once this optimal position is found we will assess the temperature and SAR underestimation of the other temperature probe positions in relation to the optimal position. In additions to the underestimation, we estimate the associated error for temperature and SAR measurement for all temperature probe positions using a numerical model of the lead.

2. Materials and methods

2.1. Experimental model

A PVC phantom (a $28 \times 20 \times 26\,\text{cm}^3$ box) was filled with 2% hydroxy-ethyl-cellulose (HEC), 0.36% sodium chloride and the rest water: a gel saline solution with 0.59 Sm^{-1} conductivity and 79 permittivity at 64 MHz, and 4178.3 J kg^{-1} K^{-1} heat capacity (ASTM 2004). A $26 \times 18\,\text{cm}^2$ grid was submerged in the gel to support the pacemaker and its lead and

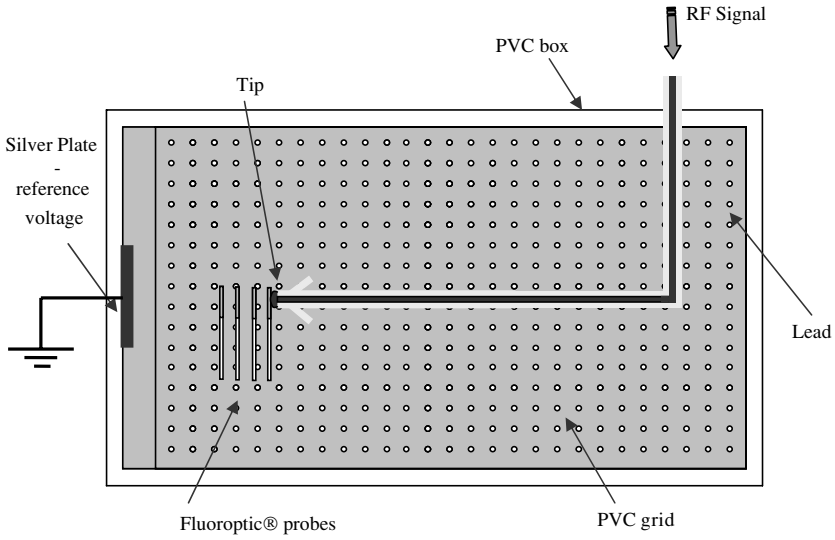

Figure 1. Experimental set-up for SAR and temperature measurements. The position of the fluoroptic® probes for model identification is also illustrated.

maintained a consistent separation distance between the implant, phantom gel surface and the temperature probes. The grid was adjusted so that the top of the implant was positioned below the phantom surface.

SAR and temperature were measured on the tip of a 62 cm long monopolar lead (S80TM, Sorin Biomedica CRM, Italy). The lead has an inner conductive wire of 0.4 mm radius, 0.5 mm external silicon insulation and a tip area of about 2 mm^2. A radio frequency (RF) signal was injected into the lead tip using a coaxial cable connected to the lead. The outer conductor (signal ground) was connected to a $1 \times 20 \times 10$ mm^3 silver plate located on one side of the PVC box. The current flow through the gel went from the lead tip to the plate (figure 1).

The lead was placed in the gel 5 cm below the phantom top surface, simulating an implant in the human body. The distance between the silver plate and the lead tip was 7 cm; the overall submerged lead length was 58 cm. Temperature was measured using a fluoroptic® thermometer (Luxtron, Model 3100, USA, SMM probes), with a resolution of 0.1 °C, operating at eight samples per second.

Three sinusoidal excitations were studied: 25, 64 and 128 MHz, which approximately correspond to the RF field used in 0.5, 1.5, and 3 T MRI systems. Signals were generated by a RF generator (Rhode & Schwartz, SMT 06), and then amplified (RFPA, RF 06100-6, France); a power meter (Rhode & Schwartz NRT, Z14, range 25–1000 MHz) was connected to the output of the amplifier measuring the average power generated and the reflection coefficient of the load.

The preliminary measurements investigated different contact configurations between the terminal part of the temperature probes and the pacing electrode at the lead tip. The aim was to identify the temperature probe position which results in the maximum heating and to assess the relative underestimations associated with other configurations.

We studied the following possibilities (figure 2):

(a) transversal contact between the side of the temperature probe and the circular surface of the lead tip;

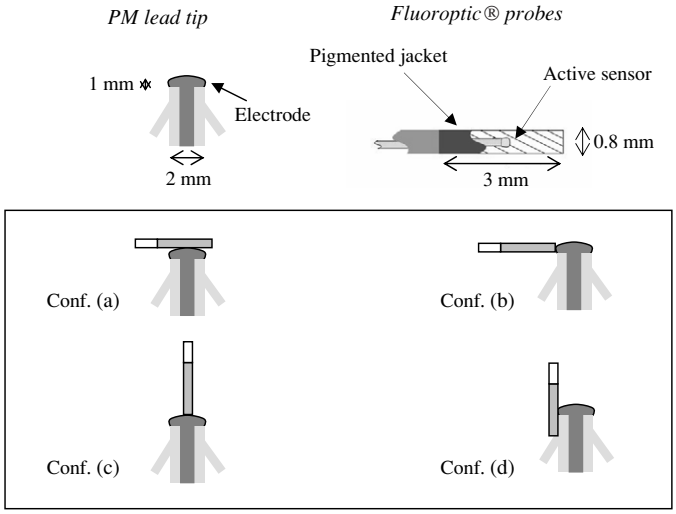

Figure 2. Schematic representation of the sensitive portion of temperature probes and different contact configuration with the tip of a pacemaker lead: transversal contact between the side of the probe and the circular surface of the lead tip (conf. (a)); transversal contact between the tip of the probe and the side surface of the electrode (conf. (b)); axial contact between the tip of the probe and the circular surface of the lead tip (conf. (c)); axial contact between the side of the probe and the side surface of the electrode (conf. (d)).

(b) transversal contact between the tip of the temperature probe and the side surface of the electrode;

(c) axial contact between the tip of the temperature probe and the circular surface of the lead tip;

(d) axial contact between the tip of the temperature probe and the side surface of the electrode.

The underestimation was expressed as the difference of the temperature increase measured with the particular temperature probe position with respect to that leading to the maximum temperature increase.

For the same experimental set-up we mapped the temperature in the HEC solution at the gel to electrode interface, at 2 mm, 4 mm and 6 mm from the lead tip (figure 1). Temperature variations were recorded for an interval of 300 s, in which the excitation was active, and in the following 200 s, with no current through the PM lead. These measurements were used to validate the numerical model described in the next section. The best fitting between experimental and modelling data was reached leaving the voltage applied on the lead tip as a free parameter.

2.2. Numerical model

A numerical model was developed to estimate the maximum temperature increase and the local SAR deposition. We used the models also to assess the measurement error due to temperature probe positioning and physical dimensions. Given the complexity of solutions for the heat-transfer thermal equations (Chang 2003, Solazzo *et al* 2005), a finite-element analysis was performed instead of an analytic solution. We developed a three-dimensional

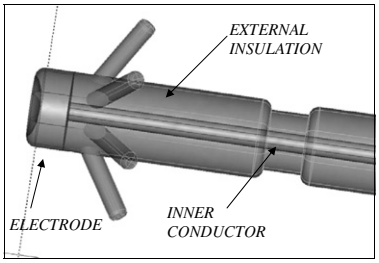

Component	Material	Electrical Conductivity [Sm^{-1}]	Thermal Conductivity [$Wm^{-1}K^{-1}$]
Electrode	Aluminum-Pyrolytic Carbon	3.77×10^{7}	0.1
External Insulation	Silicon	1×10^{-12}	163
Inner Conductor	Aluminum	3.77×10^{7}	160

Figure 3. Pacemaker lead tip: geometry and properties of the materials.

model with a commercial software (FEMLAB 3.1, Comsol Multiphysics) by which we did coupled analysis that involved simultaneously both thermal and electromagnetic equations.

The native 3D drawing section of the software was used to develop a realistic computer model of the pacemaker lead tip (figure 3). The lead tip is placed inside a saline-filled cylinder of 5 cm radius and 10 cm height). Electromagnetic and thermal properties (specific weight, heat capacity, thermal conductivity and electrical conductivity) of the different elements were chosen to closely approximate those of our experimental system.

The software is furnished with a variable grid (graded-mesh) generator. The mesh used for the finite-elements analysis was finer at the boundaries of the different domains, particularly near the lead tip (minimum cell length: 0.1 mm; element growth rate: 1.35; total number of elements: 156 775), and coarser in the homogeneous areas, to limit the complexity of the model.

To evaluate the temperature field around the lead tip, we did an electrostatic analysis, in which the model was excited by a dc voltage between the pigmented portion of the pacemaker electrode and one boundary side of the external domain, which was set at a reference voltage. This excitation simplifies the complexity of the numerical model, inducing a significant increase in spatial resolution.

The electromagnetic equations were coupled with heat-transfer thermal equation through the heat source term Q, according to the relation

$$Q = \frac{1}{2\rho} |E|^2 \sigma, \tag{1}$$

where E (V m^{-1}) is the electric field in the gel domain, ρ is the density (kg m^{-3}) of the gel and σ the electrical conductivity (S m^{-1}).

The simulation lasted 500 s, with a time step of 10 s and an initial heating phase of 300 s, followed by a 200 s period in which the voltage excitation was turned off. The time required to complete the simulation was about 3 h. We then used the numerical model to evaluate the error associated with temperature measurement using the temperature probes. Since the active temperature sensor is approximately a 0.3 mm diameter half-sphere encapsulated somewhere inside a polymer pigmented jacket which represents the terminal part of the fluoroptic® probe (figure 2), we calculated the average (ΔT_{probe}) and the maximum ($\Delta T_{\text{probe,max}}$) temperature increase in the volume covered by this jacket (cylindrical region:

radius 0.4 mm, length 3 mm), as well as the maximum temperature increase in the whole domain (ΔT_{max}). The error was quantified as

$$\Delta\text{TLE\% (`\% Local error') : } \frac{\Delta T_{probe} - \Delta T_{probe,max}}{\Delta T_{probe,max}} \times 100 \tag{2}$$

$$\Delta\text{TME\% (`\% Maximum error') : } \frac{\Delta T_{probe} - \Delta T_{max}}{\Delta T_{max}} \times 100. \tag{3}$$

ΔTLE quantifies the error due to the temperature gradient in the area covered by the pigmented portion of the temperature probe, regardless of the actual maximum temperature over the whole domain. ΔTME quantifies the error with respect to the actual maximum temperature increase in the whole domain.

2.3. SAR estimation

With the experimental data obtained with the fluoroptic® probes we could estimate the local SAR by calculating the slope (dT/dt) of the initial temperature increase, following the method indicated in the IEEE C95.3-2002 (IEEE 2002). Such procedure leads to uncertainties of about $\pm$1–2 dB in the local SAR evaluation.

The slope of the interpolating line was estimated by minimizing the R-error over about 40 samples; this estimation was assumed valid when the Pearson coefficient r^2 was greater than 0.98.

In the numerical model, the SAR was estimated by calculating the initial dT/dt of the average temperature increase on the volume of the terminal pigmented part of the temperature probe. Over a period of 10 s, with a time step of 0.1 s, SAR was calculated by minimizing the R-error over about 40 samples.

The SAR error was calculated using the same procedure as for the temperature: in the numerical model the SAR was estimated for the maximum local SAR and the mean SAR in the volume covered by the temperature probes (calculated respectively from the maximum and the mean temperature increase). The percentage measure error associated with different temperature probe positions is expressed as follows:

$$\text{SLE\% (`\% Local error') : } \frac{SAR_{probe} - SAR_{probe,max}}{SAR_{probe,max}} \times 100 \tag{4}$$

$$\text{SME\% (`\% Maximum error') : } \frac{SAR_{probe} - SAR_{max}}{SAR_{max}} \times 100, \tag{5}$$

where $SAR_{probe,max}$, SAR_{probe}, SAR_{max} are the values of SAR calculated from the maximum temperature increase in the area covered by the temperature probe, from the average temperature rise in the same area, and from the maximum temperature increase in the whole domain, respectively.

3. Results

3.1. Influence of temperature probe positioning on temperature and SAR underestimation

Figure 4 shows the pacemaker lead tip temperature increases measured with four temperature probes in different positions. The three graphs refer to 25 MHz, 64 MHz and 128 MHz, with an average net power of 0.7 W, 1.36 W and 2.04 W, respectively. These power levels

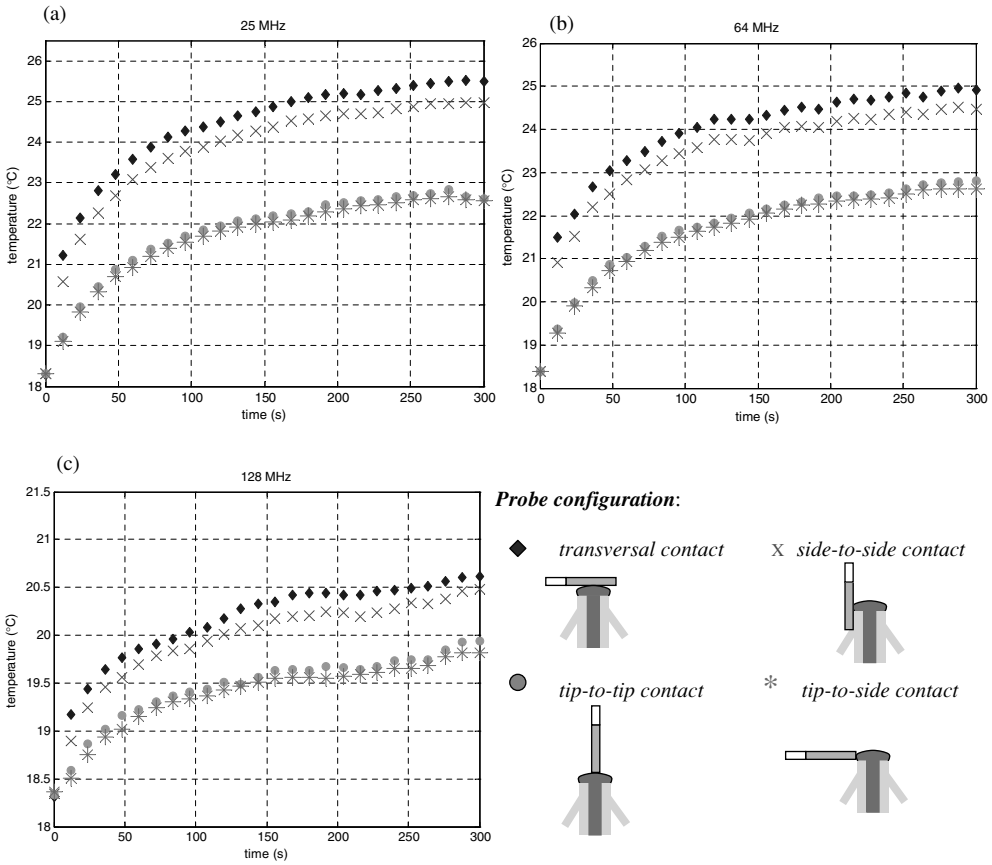

Figure 4. Temperature rise measured by temperature probes in different positions: transversal contact (diamonds); side-to-side contact (x-marks); tip-to-tip contact (dots); tip-to-side contact (stars). Frequency excitation signal: 25 MHz (a), 64 MHz (b), 128 MHz (c). Before each measurement, fluoroptic® probes were calibrated and the initial temperature was the same for all the probes.

were chosen to obtain heating comparable to those reported in the literature (Dumoulin *et al* 1993, Leung *et al* 1995, Kanal *et al* 2002, Niehaus and Tebbenjohanns 2001). A detailed investigation of the effect of the frequency on the amount of heating, for a given power, was not attempted since it was not relevant to the aim of this study.

We found that the position of the temperature probe significantly affects the measurement: transversal contact between the side of the temperature probe and the circular surface of the lead tip (figure 2(a)) is the configuration which leads to the highest measured temperature. We define the temperature measured with other positions than that leading to the maximum value as an underestimation (figure 5). The highest temperature underestimation was obtained at 25 MHz and it decreases as the frequency increases, regardless of the temperature probe contact. The configurations 'tip-to-side' (figure 2(b)) and 'tip-to-tip' (figure 2(c)) resulted in temperature underestimation ranging from 28% to 39%. The underestimation associated with the side-to-side contact was significantly lower (4–7%).

The underestimation associated with the estimation of local SAR at the lead tip showed a similar behaviour: transversal contact between the side of the temperature probe and the circular surface of the lead tip (figure 2(a)) is the configuration measuring the highest SAR

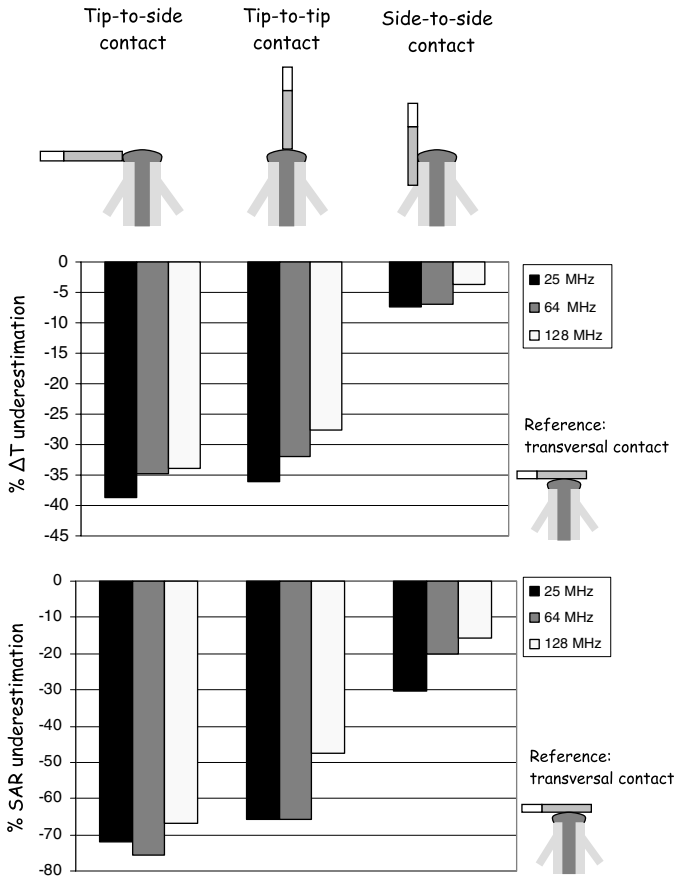

Figure 5. Underestimation: comparison among measurements made by a temperature probe in transversal contact with the active pacemaker lead (conf. (a)) and underestimation obtained with other contact configurations (conf. (b), (c), (d)): temperature and SAR comparison.

(1444 W kg^{-1}). The underestimation associated with other temperature probe configurations is reported in figure 5, lower panel. In the worst case, the SAR underestimation can be up to 75%. The effect of the frequency on SAR underestimation was similar to that observed for the temperature.

3.2. Validation of the thermal model

For best fitting with experimental measurements at 25, 64 and 128 MHz we applied on the pacemaker lead tip a voltage of 7, 11.5 and 12 V, respectively. Figure 6 shows the numerical and experimental data. The excitation was active for 300 s following by a 200 s cooling phase. We positioned the temperature probes in transversal position with the lead at 2 mm, 4 mm and 6 mm from the tip (solid lines). The computed temperature distribution was sampled at the same position of the pigmented portions of the temperature probes. For each of these positions we then calculated the average temperature over the volume covered by the pigmented portions of the temperature probes.

The numerical results reproduced the temperature increase measured at 25 and 64 MHz. For each temperature curve, the difference between experimental and numerical results was

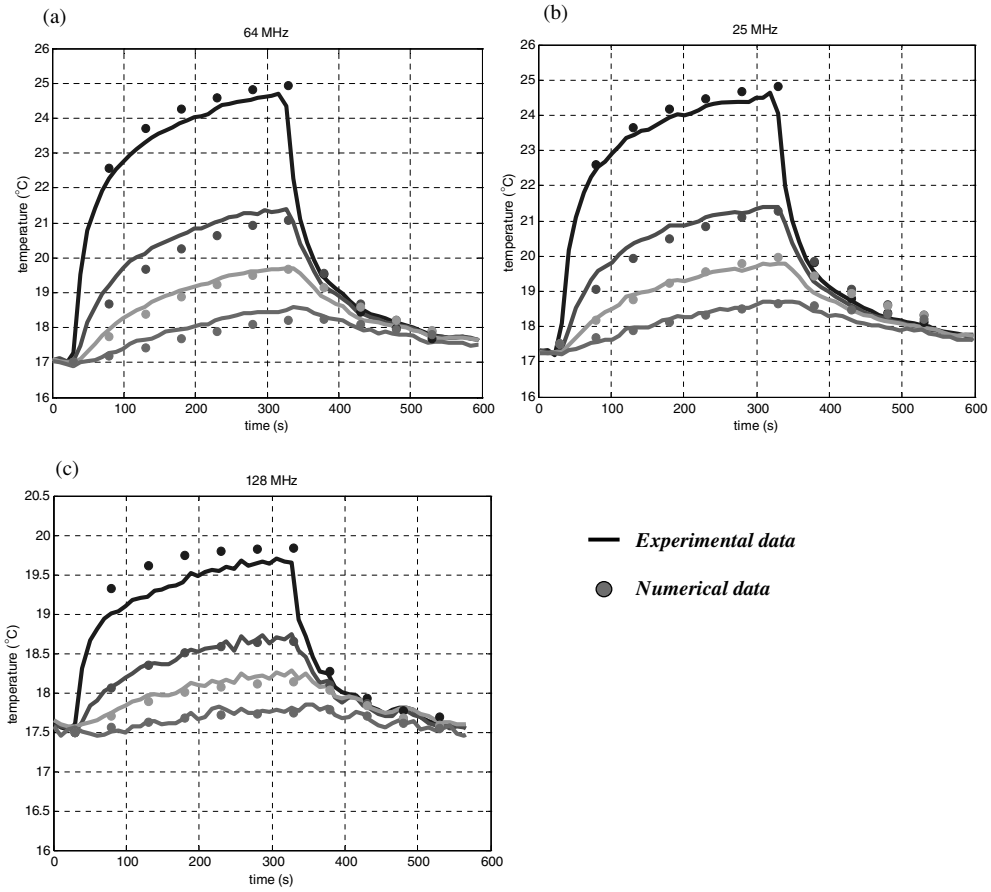

Figure 6. Validation of the model: experimental data (solid lines) were compared with temperature distributions from computer simulations (dots). Excitation signal was set at 25 MHz (a), 64 MHz (b) and 128 MHz (c). For each frequency, heat distribution was characterized by sampling temperature at the lead surface and at 2 mm, 4 mm and 6 mm from the tip. Note that temperature scale of panel (c) differs from the others.

within the resolution of the fluoroptic® temperature probes (0.1 °C), in both the heating and cooling phase. The numerical model also showed a good agreement with experimental data in terms of spatial distribution of the temperature field: at each distance the difference between experimental and numerical results was comparable for all temperature probes. At 128 MHz the numerical model showed a poorer fitting of the temperature rise, even though at the end of the heating phase the spatial distribution of the temperature was in agreement with the experimental data.

3.3. Influence of temperature probe positioning on temperature and SAR error

As illustrated in figure 7, the spatial temperature gradient around the lead tip was very high, which indicates that the physical dimension of the temperature probes may not be neglected. The measurement error was related to the positioning of the terminal portion of the temperature probes in which the active sensor is encapsulated and which covers a volume with large spatial temperature gradients. The values of the local and maximum temperature and SAR errors are reported in figure 8. The transversal contact between the temperature probe and the

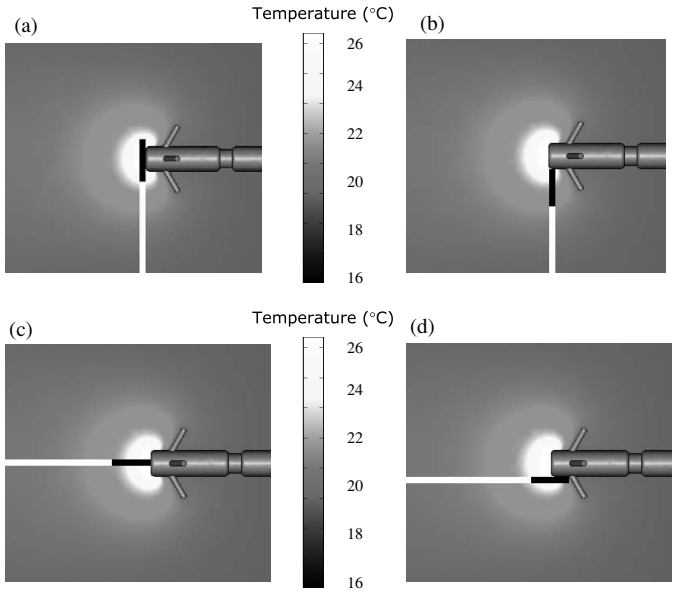

Figure 7. Temperature field resulting from the numerical model. The different contact configurations for the probes are also shown: (a) transversal contact; (b) tip-to-side contact; (c) tip-to-tip contact; (d) side-to-side contact. Temperature grey-map is valid only for the gelled domain, but not for the probes and the lead.

pacemaker lead tip, which lead to the lowest temperature and SAR underestimation, is also the configuration associated with the lowest maximum errors, both for temperature and SAR measurements. The maximum error in the measurement of temperature increase (-45%, absolute error: $-4\ ^{\circ}\mathrm{C}$) was yielded by the tip-to-side contact, while the positioning resulting in the lowest underestimation (transversal contact) also resulted in the lowest error, i.e., -10% or as absolute error $-0.9\ ^{\circ}\mathrm{C}$.

The error associated with SAR measurement was higher than those of temperature (range -30 to 54%); in addition, the positioning of the temperature probes played a minor role for the SAR error. The transversal contact was always the configuration associated with the lowest maximum SAR error (percentage error: -41%, absolute error: $-1069\ \mathrm{W\ kg^{-1}}$).

4. Discussion

Using temperature measurements on a physical model of a pacemaker lead we found that the positioning of temperature probes strongly affects temperature and SAR results. Due to the comparable dimension of the temperature probes with the pacing electrode and due to the large spatial temperature gradient around the lead tip, temperature probes tend systematically to underestimate the real value of local temperature and SAR. In particular, using the SMM Luxtron fluoroptic® probes, we found that a transversal contact of the temperature probe with the lead tip always gives the highest temperature and SAR values. Such a result points out that the active sensor is likely to occupy the central region of the pigmented jacket of the temperature probe. Assuming this configuration as reference, the underestimation yielded by other configurations may be as high as 39% for temperature and 75% for SAR.

The experiments allowed us to identify the temperature probe configuration for measuring the highest temperature increase but could not give us the temperature and SAR error. Since the active temperature sensor is placed somewhere inside the terminal pigmented portion of the

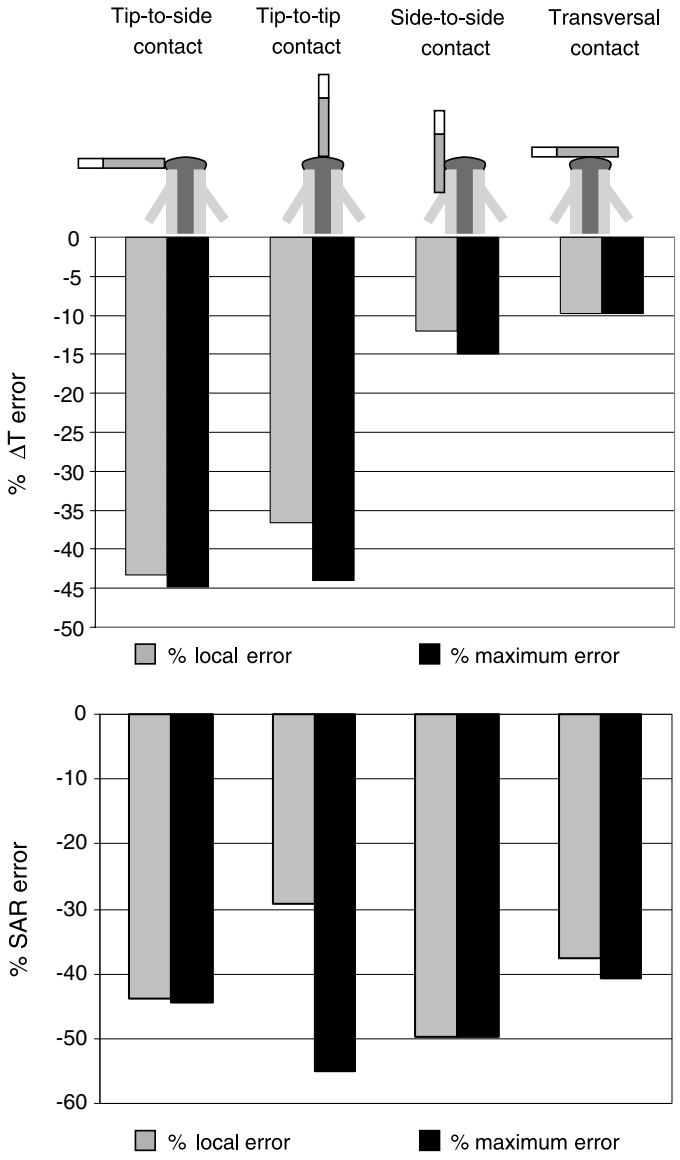

Figure 8. Numerically calculated error associated with temperature increase and SAR measurements obtained from fluoroptic® probes. For each contact configuration the error is expressed in terms of local error (referred to the highest temperature in the area covered by the pigmented portion of the probe) and maximum error (referred to the highest temperature in the whole domain).

probe, which covers an area with significant temperature gradients, the measured temperature needs to be averaged over the pigmented jacket. Therefore we developed a numerical model to quantify this error. The model was validated by comparing the numerical results with the experimental measures obtained with fluoroptic® probes in the transversal contact configuration, at 2, 4 and 6 mm from the lead tip. With this configuration we characterized both time and space distribution of the temperature. Due to the physical dimensions of the lead and the spatial resolution, required for consistent temperature estimation, Maxwell's equations

were solved under electrostatic approximation. The correspondence between experimental and numerical data was confirmed at 25 and 64 MHz in both the time-transient heating and cooling phases. The spatial distribution of the temperature showed good agreement with the data sampled at various distances from the tip (0, 2, 4, 6 mm). The worst fitting was obtained at 128 MHz, specifically in the dynamical rise of temperature. This suggests that the heat generation at 128 MHz begins to be affected by displacement currents.

Simulated results are consistent with experimental data: the temperature gradient around the lead tip is high enough that the physical dimensions of the temperature probes must not be neglected. As a consequence, the measurement of the temperature increase is always too low. In the best case (transversal contact) the maximum error is about -10%, but can be as high as -45% in the worst case (tip-to-side contact).

The error associated with the measurement of local SAR is higher than the temperature error. SAR is calculated as the slope of the initial linear temperature increase and is therefore affected by the spatial distribution of the temperature in the first instants of the heat generation process. Thus, the effect of the dimensions of the physical probe is higher than at steady state. After about 300 s the temperature distribution became more homogenous, consequently reducing the error. In agreement with experimental data, the SAR error is also less sensitive to probe positioning than temperature measures. The maximum error for SAR is about -40% for the transversal contact position but can go up to -54% for the tip-to-tip contact. Also, the temperature probe position leading to the lowest underestimation has the lowest error for temperature and SAR measurements as well.

The physical model adopted in this work reproduced the lead tip heating but not the current-induction of an MRI system. Future analysis could be extended to pacemaker lead tip temperature measurements with temperature probes during real MRI systems. Furthermore, thermal events at the tip of a pacemaker lead are the same for all linear conductive structures with comparable dimensions; this fact suggests the possibility of extending the results of this work to other medical devices commonly used under MRI guidance, such as guide wires and catheters in interventional therapy.

In addition, our data show a frequency dependence of the underestimation in temperature and SAR measurements. The aim and the design of our study do not allow an explanation of this phenomenon. Such an explanation would require a deeper and dedicated analysis, which was beyond this study.

The investigation of the temperature and SAR errors yielded by other fluoroptic® probe types, such as surface and remote style probes, was beyond the aim of this paper. The SMM probes were chosen because they can guarantee a reliable contact even with very thin wires. In addition, since heating is generated at the interface between metallic structure and gel, surface contact probes would not be located in the actual hot spot area.

5. Conclusions

The results showed the sensitivity of these measurements on temperature probe contact positioning. The transversal contact of the pigmented portion of the temperature probe and the lead tip minimized the underestimation for temperature and SAR and therefore gave always the highest values for this type of pacemaker lead. Other contact configurations may cause a temperature underestimation of up to 39% and a SAR underestimation of up to 75%. For all contact configurations the transversal contact showed the lowest maximum temperature error (-10%) and the lowest maximum SAR error (-40%). The maximum temperature error can be as high as -45% for the tip-to-side configuration whereas the maximum SAR error is highest for the tip-to-tip configuration (-54%). For all MRI heating evaluations

with temperature probes, a contact position leading to the lowest maximum error should be used and the error should be specified. Scientific sound MRI heating evaluations need to be accompanied by a thorough uncertainty budget. Therefore, other uncertainty factors should also be evaluated when specifying temperature and SAR values on implants based on measurements with fluoroptic® temperature probes.

6. Disclaimer

The opinions and conclusions stated in this paper are those of the authors and do not represent the official position of the Department of Health and Human Services. The mention of commercial products, their sources, or their use in connection with material reported herein is not to be construed as either an actual or implied endorsement of such products by the Department of Health and Human Services.

Acknowledgments

Authors wish to thank Sorin Biomedica Cardio (eng. G. Gaggini) for providing the pacemakers and their leads; Monica Brocco for the linguist revision of the paper.

References

Achenbach S, Moshage W, Diem B, Bieberle T, Schibgilla V and Bachmann K 1997 Effects of magnetic resonance imaging on cardiac pacemakers and electrodes *Am. Heart J.* **134** 467–73

American Society for Testing and Materials (ASTM) 2004 Standard test method for measurement of radio frequency induced heating near passive implants during magnetic resonance imaging *ASTM Designation*: F2182-02a

Atalar E, Kraitchman D L, Carkhuff B, Lesho J, Ocali O, Solaiyappan M, Guttman M A and Charles H K Jr 1998 Catheter-tracking FOV MR fluoroscopy *Magn. Reson. Med.* **40** 865–72

Baker K B, Tkach J A, Nyenhuis J A, Phillips M, Shellock F G, Gonzalez-Martinez J and Rezai A R 2004 Evaluation of specific absorption rate as a dosimeter of MRI-related implant heating *J. Magn. Reson. Imaging* **20** 315–20

Blouin L T, Marcus F I and Lampe L 1991 Assessment of effects of a radiofrequency field and thermistor location in an electrode catheter on the accuracy of temperature measurement *Pacing Clin. Electrophysiol.* **14** 807–13

Chang I 2003 Finite element analysis of hepatic radiofrequency ablation probes using temperature-dependent electrical conductivity *Biomed. Eng. Online* **2** 12

Dinerman J L, Berger R D and Calkins H 1996 Temperature monitoring during radiofrequency ablation *J. Cardiovasc. Electrophysiol.* **7** 163–73

Dumoulin C L, Souza S P and Darrow R D 1993 Real-time position monitoring of invasive devices using magnetic resonance *Magn. Reson. Med.* **29** 411–5

Glowinsky A, Adam G, Brücker A, Neuerburg van J, Vaals J J and Günther R W 1997 Catheter visualization using locally induced, actively controlled field inhomogeneities *Magn. Reson. Med.* **38** 253–8

IEEE 2002 Recommended practice for measurements and computations with respect to human exposure to radiofrequency electromagnetic fields, 100 kHz to 300 GHz *IEEE Standard* C95.3-2002 (Institute of Electrical and Electronics Engineers)

Kanal E *et al* 2002 American College of Radiology white paper on MR-safety *Am. J. Roentgenol.* **178** 1335–47

Leung D A, Debatin J F, Wildermuth S, McKinnon G C, Holtz D, Dumoulin C L, Darrow R D, von Hofmann E and Schulthess G K 1995 Intravascular MR tracking catheter: preliminary experimental evaluation *Am. J. Roentgenol.* **164** 1265–70

Niehaus M and Tebbenjohanns J 2001 Electromagnetic interference in patients with implanted pacemakers or cardioverter-defibrillators *Heart* **86** 246–8

Nitz W R, Oppelt A, Renz W, Manke C, Lenhart M and Link J 2001 On the heating of linear conductive structure as guide wires and catheters in interventional MRI *J. Magn. Reson. Imaging* **13** 105–14

Pinski S L and Trohman R G 2002 Interference in implanted cardiac devices: part II. *Pacing Clin. Electrophysiol.* **25** 1496–509

Roguin A, Zviman M M, Meininger G R, Rodrigues E R, Dickfeld T M, Bluemke D A, Lardo A, Berger R D, Calkins H and Halperin H R 2004 Modern pacemaker and implantable cardioverter/defibrillator systems can be magnetic resonance imaging safe. In vitro and in vivo assessment of safety and function at 1.5 T *Circulation* **110** 475–82

Ruggera P S, Witters D M, von Maltzahn G and Bassen H I 2003 *In vitro* assessment of tissue heating near metallic medical implants by exposure to pulsed radio frequency diathermy *Phys. Med. Biol.* **48** 2919–28

Shellock F G 1992 Thermal responses in human subjects exposed to magnetic resonance imaging *New York Acad. Sci.* **649** 260–72

Shellock F G and Crues J V III 2002 MR-safety and the American College of Radiology white paper *Am. J. Roentgenol.* **178** 1349–52

Shellock F G, Schaefer D J and Kanal E 1994 Physiologic responses to an MR imaging performed at a specific absorption rate of 6.0 W/kg[1] *Radiology* **192** 865–8

Shellock F G and Shields C L Jr 2000 Radiofrequency energy-induced heating of bovine articular cartilage using a bipolar radiofrequency electrode *Am. J. Sports Med.* **28** 720–4

Solazzo S A, Liu Z, Lobo S M, Ahmed M, Hines-Peralta A U, Lenkinski R E and Goldberg S N 2005 Radiofrequency ablation: importance of background tissue electrical conductivity—an agar phantom and computer modeling study *Radiology* **236** 495–502

Sommer T *et al* 2000 MR imaging and cardiac pacemakers: in-vitro evaluation and in-vivo studies in 51 patients at 0.5 T *Radiology* **215** 869–79

Wickersheim K A and Sun M H 1987 Fluoroptic® thermometry *Med. Electron. (February)* 84–91